*Desalination and Water Treatment*
www.deswater.com

doi: 10.5004/dwt.2020.26378

207 (2020) 233–245
December

# Succinic anhydride modified multi-walled carbon nanotubes encapsulated in polymeric gel with enhanced trapping performance for metal ions removal

Lingyun Jing[a,*], Ting Zhang[a], Xia Zhao[a], Xiaoning Jia[a], Gang Xie[a], Tao Yu[a], Jianrong Chen[b], Bin Yao[b]

[a]*School of Petrochemical Engineering, Lanzhou University of Technology, Lanzhou 730050, China, emails: jingly12@lzu.edu.cn (L.Y. Jing), zhangting@lut.edu.cn (T. Zhang), zhaoxia@lut.cn (X. Zhao), , jxn422@163.com (X.N. Jia), xiegang@lut.edu.cn (G. Xie), 282149462@qq.com (T. Yu)*
[b]*Research Institute of Water and Soil Conservation of Gansu Province, Lanzhou 730000, China, emails: chenjianrong_lz@163.com (J.R. Chen), 994316937@qq.com (B. Yao)*

Received 8 February 2020; Accepted 22 July 2020

**ABSTRACT**

Novel composites of succinic anhydride modified multi-walled carbon nanotubes (MWCNTs), that is, MWCNTs-NC, encapsulated in macroporous poly(vinyl alcohol) (PVA) have been successfully developed with excellent $Pb^{2+}$ and $Cu^{2+}$ adsorption performance. It was found that nearly 100% of $Pb^{2+}$ and 72% of $Cu^{2+}$ could be removed by PVA/MWCNTs-NC at a wide pH range. It was revealed by Fourier-transform infrared spectroscopy and X-ray photoelectron spectroscopy that the adsorption mechanism was mainly the chemical binding that occurred between functional groups derived from succinic anhydride and metal ions. Moreover, adsorption experiments were conducted in the fixed-bed continuous-flow column system to further evaluate the potential application of PVA/CNTs-NC for heavy metal ions removal.

*Keywords:* PVA/MWCNTs-NC; $Pb^{2+}$; $Cu^{2+}$; Succinic anhydride; Continuous-flow column

## 1. Introduction

$Pb^{2+}$ and $Cu^{2+}$ contamination in effluents discharged from various industrial and agricultural activities has been a serious environmental threat due to its high toxicity even at very low concentrations [1–3]. During the past decades, several techniques have been developed in the removal of $Pb^{2+}$ and $Cu^{2+}$ from the wastewater among which adsorption is considered to be one of the most effective approaches due to low-cost, easy operation and good performance [4–6].

Multi-walled carbon nanotubes (MWCNTs) based materials have been widely used in wastewater treatment because of their high surface area, hollow nanosized structure and chemical stabilities [7–9]. One way to enhance the adsorption performance is to introduce more active sites on the surface of MWCNTs through surface modification [10,11]. Previously reported adsorbents such as MWCNTs – phenyl – iminodiacetic acid, MWCNTs – 2-aminobenzothiazole, MWCNTs – tris(2-aminoethyl)amine and MWCNTs – ethylenediamine and humic acid (HA)-MWCNTs showed the adsorption capacities up to 333 and 30.5 mg/g for Pb(II) and Cu(II), respectively using batch methods [12–15]. In spite of the enhanced adsorption capacities, these functionalized MWCNTs were still difficult to separate and/or diffuse well in aqueous solutions, which is a severe obstacle to application in wastewater treatment because the nanoparticles such as MWCNTs tend to aggregate into large particles leading to the deteriorated adsorption capacities [16,17]. Moreover, it is challenging to use these functionalized MWCNTs directly in the fixed bed reactor. To avoid these

* Corresponding author.

problems, it would be a promising way to use porous materials as the matrix to disperse and immobilize MWCNTs [18,19]. The well-dispersed MWCNTs with a high content in the porous matrix would be of great benefit to the fabrication of adsorbents for Pb(II) and Cu(II) removal.

In this work, macroporous poly(vinyl alcohol) (PVA) with large pores (>100 nm) and high pore volumes were chosen as the porous matrix to encapsulate succinic anhydride modified MWCNTs (MWCNTs-NC). After modification, there would be more active sites (amine and carboxylate groups) on the surface of MWCNTs leading to high adsorption capacity and rapid adsorption rate. On the other hand, embedding MWCNTs-NC into PVA would add additional properties of this composite material such as easy separation and good reusability. The adsorption performance of $Pb^{2+}$ and $Cu^{2+}$ on MWCNTs-NC and PVA/MWCNTs-NC was studied in detail. Fourier-transform infrared spectroscopy (FTIR) and X-ray photoelectron spectroscopy (XPS) techniques were used to elucidate the possible adsorption mechanisms of $Pb^{2+}$ and $Cu^{2+}$ on PVA/MWCNTs-NC. Moreover, the adsorption of $Pb^{2+}$ and $Cu^{2+}$ on PVA/MWCNTs-NC in a fixed-bed continuous-flow column was further studied for the potential practical application.

## 2. Materials and methods

### 2.1. Chemicals and reagents

PVA (polymerization degree: 1,750; alcoholysis degree: >99%) was purchased from Lanzhou Vinylon Factory (Gansu, China). Hydroxy purified MWCNTs (outer diameter: 10–20 nm; inner diameter: 5–10 nm; length: 10–30 μm; –OH content: 3.06%) were purchased from Chengdu Organic Chemicals Co., Ltd., (Sichuan, China). All other chemicals were of analytical reagent grade.

### 2.2. Preparation of PVA/MWCNTs-NC

MWCNTs-NC was prepared as follows: the schematic drawing of the synthesis approach was shown in Fig. 1. 5.0 g of MWCNTs and 160 mL of toluene were added to a three-neck round-bottom flask equipped with a reflux condenser

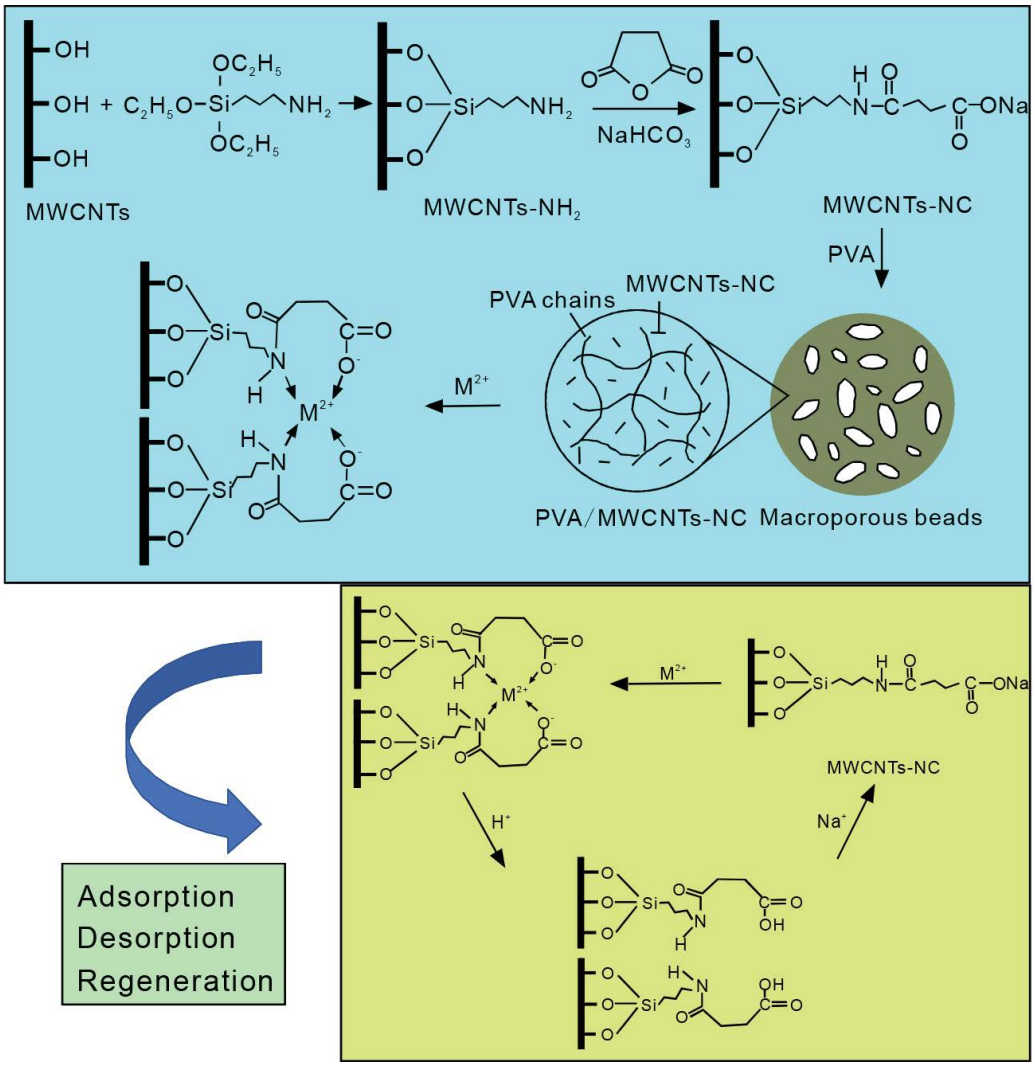


Fig. 1. A synthesis scheme of MWCNTs-NC and PVA/MWCNTs-NC and possible generation route.

and an automatic stirrer. The flask was kept in an ultrasonic bath for 10 min. 8.0 mL of (3-aminopropyl)triethoxysilane (APTES) was dropwise added into the flask and kept at 65°C–75°C under stirring for 24 h. Then, 120 mL of N,N-dimethylformamide (DMF) was added into the flask and stirred for 1 h. After that, succinic anhydride was added into the solution with stirring at 65°C–75°C for 24 h. The obtained material was centrifuged and thoroughly washed with DMF, anhydrous ethanol, saturated $NaHCO_3$ and distilled water. Saturated $NaHCO_3$ was used to convert the carboxylic acid into carboxylate ions. As a result, MWCNTs-NC was obtained.

PVA/MWCNTs-NC was prepared as follows 6.0 g of PVA, 1.3 g of sodium alginate and 7.5 g of $CaCO_3$ were added to a flask containing 80 mL of distilled water and kept at 90°C–100°C under stirring for 2 h. Then 1.0 g of MWCNTs-NC was added to 20 mL of cetyltrimethylammonium bromide solution (0.5% w/w in distilled water). The obtained solution was kept in an ultrasonic bath for 5 min before adding to the PVA/$CaCO_3$ mixture which was stirred at 90°C for another 6 h. The obtained gel was dropped into the saturated boric acid solution containing 3% (w/v) of $CaCl_2$ by using a syringe. The black crosslinked beads formed instantaneously and were kept in the solution for 48 h. At last, 1 mol/L of HCl was added into the solution to form porous beads.

### 2.3. Characterization

The FTIR spectra of PVA/MWCNTs-NC before (non-loaded) and after adsorption ($Pb^{2+}$ and $Cu^{2+}$ loaded) were obtained (NEXUS 670, Nicolet, USA) in the range of 4,000–500 $cm^{-1}$ using KBr pellets. X-ray diffraction (XRD) patterns of all samples were recorded with a D/Max-2400 instrument (Rigaku, Japan) using Cu $K_\alpha$ radiation at 40 kV and 40 mA over the range (2θ) of 5°–70°. Elemental analysis (CHN) was performed using a PerkinElmer model 2400 CHN analyzer (USA). XPS was employed to investigate the adsorption mechanisms. The surface area, total pore volume and average pore diameter were determined by $N_2$ adsorption using Autosorb (Quantachrome Corp., USA). The Brunauer–Emmett–Teller (BET) surface area was obtained by applying the BET equation to the adsorption data. $V_{tot}$ was obtained from the adsorption at $P/P_0$ = 0.96. Scanning electron microscopy images were performed with an electron microscope (HITACHI S-4800, Japan). The accelerating voltage was 15.00 kV and the scanning was performed *in-situ* on a sample powder.

### 2.4. Adsorption experiments

Stock solutions of $Pb^{2+}$ and $Cu^{2+}$ were prepared by dissolving an accurate quantity of $Pb(NO_3)_2$ and $CuSO_4$ in distilled water, respectively. Batch adsorption experiments were performed on a temperature-controlled shaker at 30°C and 120 rpm. The concentration of $Pb^{2+}$ and $Cu^{2+}$ was determined spectrophotometrically [20,21] by using a double beam UV-vis spectrophotometer (Shimadzu, Model UV-1601, Japan). The effect of pH on adsorption by PVA/MWCNTs-NC was studied by varying the solution pH from 2.0 to 7.0, with the initial $Pb^{2+}$ or $Cu^{2+}$ concentration of 100 mg/L. Adsorption isotherm data were generated by performing the experiment at 308 K, with the sample solution containing varying concentrations ranging from 50 to 500 mg/L. Adsorption kinetic samples were prepared by adding 0.2 g of PVA/MWCNTs-NC into a 100 mL solution with an initial concentration of 100 mg/L (pH 6.0). Samples of 0.1 mL were taken at predetermined time intervals for the analysis of $Pb^{2+}$ or $Cu^{2+}$ in the solution. The ionic strength of the solutions was adjusted to the range of 0.0008–0.17 M by adding an appropriate amount of sodium nitrate salt, then 0.2 g adsorbent and 100 mL $Pb^{2+}$ or $Cu^{2+}$ solution with diverse ionic strength were shaken for 2 h. The effect of HA on $Pb^{2+}$ and $Cu^{2+}$ adsorption was performed by varying HA concentration in the solutions from 2.0 to 10.0 mg/L, with the initial $Pb^{2+}$ or $Cu^{2+}$ adsorption of 100 mg/L.

The equilibrium metal adsorption capacity ($Q_e$) was calculated for each sample using the following expression:

$$Q_e = \frac{(C_0 - C_e)}{W} \uparrow \quad (1)$$

where $C_0$ and $C_e$ are the initial and equilibrium metal concentrations (mg/L), respectively. $V$ is the solution volume (L) and $W$ is the weight of the adsorbents (g).

### 2.5. Column adsorption experiments

The breakthrough test using PVA/MWCNTs-NC as adsorbents were carried out in a quartz column with an inside diameter of 2.5 cm and a column length of 30 cm. A known weight of PVA/MWCNTs-NC was packed in the vertical column with a bed length of 10 cm. The "up-flow" condition was applied in this experiment. The solution with a certain $Pb^{2+}$ concentration was pumped into the fixed-bed flow reactor at a flow rate of 2–4 mL/h and room temperature. The concentration of $Pb^{2+}$ in the effluent was measured at different operating times.

## 3. Results and discussion

### 3.1. Characterization of PVA/MWCNTs-NC

The FTIR spectra (Fig. 2A) revealed the chemical information and major functional groups in MWCNTs-NC and PVA/MWCNTs-NC. The sharp peaks at 3,439.8 and 1,091.0 $cm^{-1}$ (Fig. 2A(a)) corresponding to the O–H and C–O stretching vibrations in MWCNTs shifted to 3,436.1 and 1,071.1 $cm^{-1}$, respectively, after reacting with APTES. Moreover, new peaks at 2,886.5; 1,554.6 and 1,330.7 $cm^{-1}$ were assigned to C–H, N–H and C–N stretching vibrations [22], respectively, indicating that APTES was successfully grafted on the surface of MWCNTs (Fig. 2A(b)). For MWCNTs-NC, two new peaks at 1,624.5 and 1,454.8 $cm^{-1}$ could be attributed to C=O stretching in amide group (–CONH–) and carboxylate salts (–COO–), respectively (Fig. 2A(c)), suggesting that the amine groups were involved in this reaction and a large number of carboxylate groups were introduced to the surface of MWCNTs-NC. After embedding MWCNTs-NC into PVA, the width of the peak at 3,424.8 $cm^{-1}$ was obviously broadened, which could be attributed to the introduction of hydroxyl groups of PVA (Fig. 2A(d)). After $Pb^{2+}$ and $Cu^{2+}$ adsorption, peaks at 1,624.6 and 1,428.6 $cm^{-1}$ shifted slightly. The peak of C–N stretching vibration shifted to 1,330.3 and 1,326.5 $cm^{-1}$, respectively and the peak at 1,116.5 $cm^{-1}$

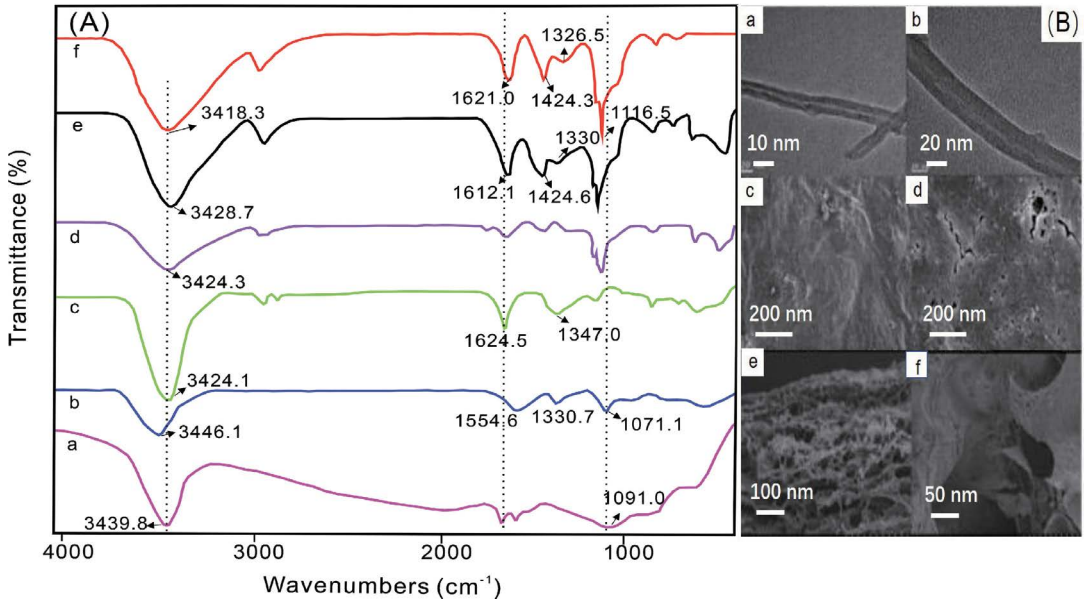


Fig. 2. (A) FTIR spectra of MWCNTs (a), MWCNTs-$NH_2$ (b), MWCNTs-NC (c), PVA/MWCNTs-NC (d) and PVA/MWCNTs-NC after $Pb^{2+}$ and $Cu^{2+}$ adsorption (e and f) and (B) transmission electron microscopy images of MWCNTs (a) and MWCNTs-NC (b) and scanning electron microscopy images of PVA/MWCNTs-NC the surface (c and d) and the cross-section (e and f).

assigned to C–OH also showed a slight change (Figs. 2A(e) and (f)). These results indicated that amide, carboxylate and hydroxyl groups may be involved in the process of metal adsorption.

As shown in Fig. 2B, surface modification of MWCNTs did not significantly change the morphologies of MWCNTs (Figs. 2B(a) and (b)). PVA/MWCNTs-NC exhibited spherical in shape with an average diameter of 3 cm and a rough surface (Fig. 2B(c)). Moreover, many macropores and micropores were unevenly distributed in the surface and interior of PVA/MWCNTs-NC (Figs. 2B(d) and (f)). It was observed that the surface area of PVA/MWCNTs-NC (Fig. 2B(e)) was much denser than the internal region, which might be attributed to the stronger chemical crosslinking established between the borate ions and hydroxyl groups on the surface of PVA/MWCNTs-NC [19]. Thus, it was demonstrated that PVA/MWCNTs-NC possessed a large number of amine and carboxylate groups, rough surface and three-dimensional network structure with well-interconnected pores, which would greatly lead to higher adsorption capacity and faster adsorption rate.

XRD pattern for MWCNTs (Fig. 3) shows a strong diffraction peak at around 26.0°, indicating the crystalline structure of MWCNTs. Three new peaks at around 22.4°, 30.4° and 34.5° were observed for MWCNTs-NC, which might be due to the introduction of amine and carboxylate groups. After MWCNTs-NC was embedded in PVA, the peak intensity of MWCNTs-NC decreased. The wide-angle XRD pattern indicated the amorphous nature of PVA/MWCNTs-NC, which might be attributed to the fact that embedding of MWCNTs-NC in PVA decreased the aggregation of MWCNTs-NC.

As can be seen from Table 1, after modification with succinic anhydride, the N content increased to 1.03% and 0.58% for MWCNTs-NC and PVA/MWCNTs-NC,

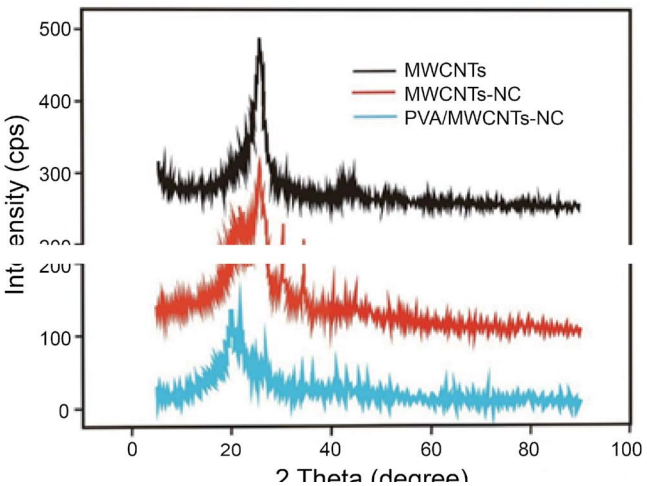


Fig. 3. XRD patterns of MWCNTs, MWCNTs-NC and PVA/MWCNTs-NC.

respectively. However, the surface area and pore volume of the MWCNTs significantly decreased, which was probably due to the blockage of the pores of the MWCNTs by surface modification.

### 3.2. Adsorption experiments

#### 3.2.1. Effect of the initial metal concentrations

As shown in Fig. 4a, chemical modification of MWCNTs with APTES and succinic anhydride greatly improved the adsorption performance for $Pb^{2+}$ and $Cu^{2+}$ removal. The maximum adsorption capacities of MWCNTs-NC for $Pb^{2+}$ and $Cu^{2+}$ were 244 and 215 mg/g, respectively, which were

Table 1
Element analysis of the obtained materials

| Sample | Element analysis | | | Surface area | Pore volume | Pore size |
|---|---|---|---|---|---|---|
| | (%) | | | ($m^2$/g) | ($cm^3$/g) | (nm) |
| | C | H | N | | | |
| MWCNTs | 98.07 | 0.655 | 0.00 | 148.73 | 0.91 | 24.41 |
| MWCNTs-NC | 94.55 | 1.057 | 1.03 | 78.65 | 0.55 | 27.86 |
| PVA/MWCNTs-NC | 55.60 | 5.406 | 0.58 | 27.76 | 0.15 | 21.81 |

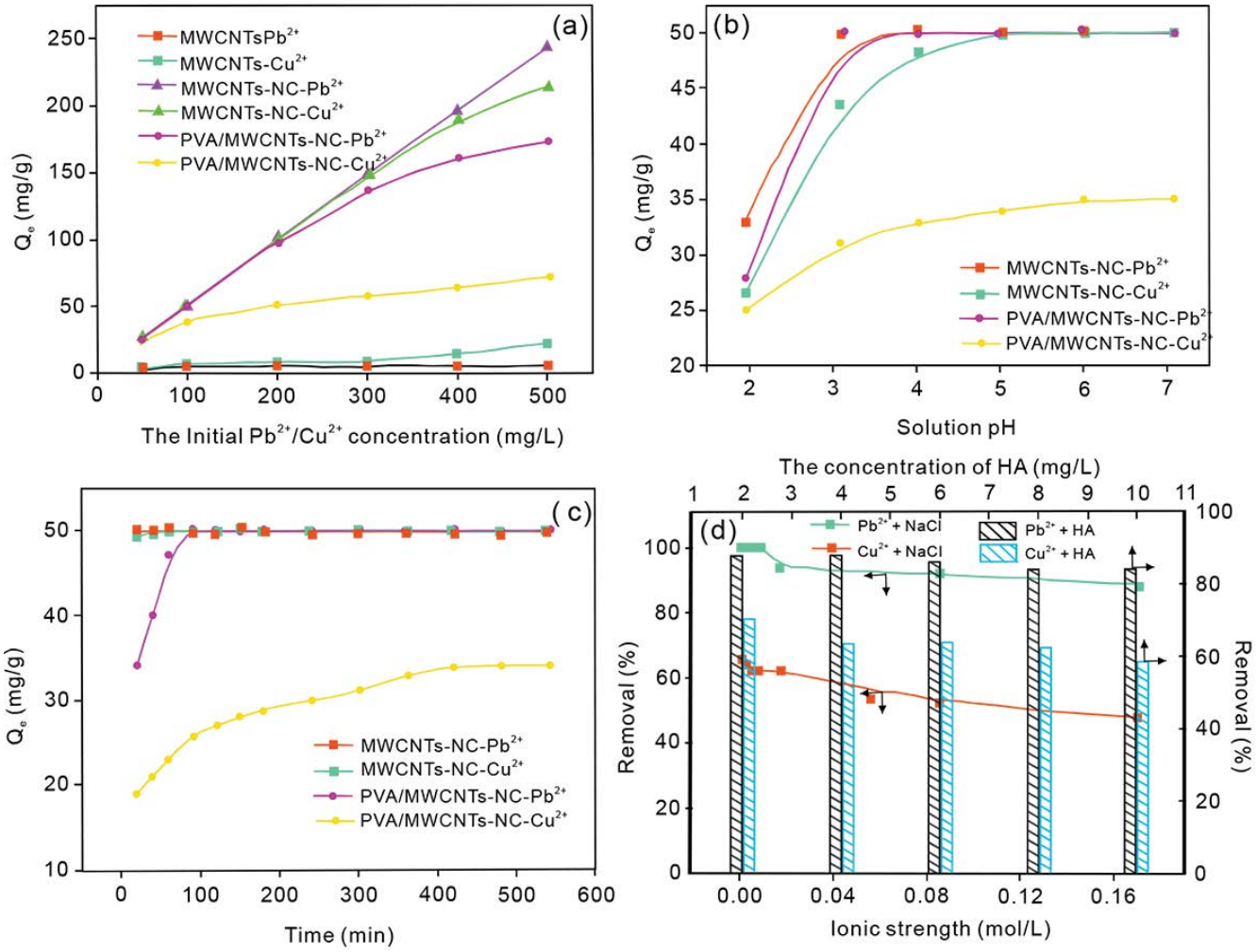


Fig. 4. Effect of initial metal concentrations, solution pH, contact time, ionic strength and HA on $Pb^{2+}$ and $Cu^{2+}$ adsorption by prepared adsorbents.

about 40 and 10 times higher than those of the unmodified MWCNTs. This might be due to the fact that a large number of amine and carboxylate groups from the functionalized MWCNTs would provide more active sites for metal ions binding. While the adsorption capacities of PVA/MWCNTs-NC for $Pb^{2+}$ and $Cu^{2+}$ were lower than those of MWCNTs-NC. It was not unexpected because MWCNTs content in PVA/MWCNTs-NC beads was lower so that less active sites for metal ions binding were provided. On the other hand, embedding MWCNTs-NC into PVA beads made the specific adsorption sites not as easily available as the pristine MWCNTs. However, PVA/MWCNTs-NC still exhibited excellent adsorption performance for $Pb^{2+}$ ions. As initial $Pb^{2+}$ concentration was lower than 100 mg/L, nearly 100% of $Pb^{2+}$ was removed by PVA/MWCNTs-NC. Moreover, the spherical adsorbents were easily separated

from the solution and appropriate for further reuse, which was especially important for continuous flow operations.

*3.2.2. Effect of initial pH*

Fig. 4b shows that MWCNTs-NC and PVA/MWCNTs-NC exhibited a very strong affinity towards $Pb^{2+}$ ions. The removal efficiency of $Pb^{2+}$ on MWCNTs-NC and PVA/MWCNTs-NC increased rapidly from 66% to 99.9% and 56% to 99.8% by changing the solution pH from 2.0 to 3.0, respectively. And then it remained almost constant with a further increase in solution pH. While the adsorption capacity of $Cu^{2+}$ onto MWCNTs-NC and PVA/MWCNTs-NC increased with the increase of solution pH from 2.0 to 4.0 and reached the maximum values at pH 6.0–7.0. This might be due to that at lower pH, a higher concentration of $H^+$ reacted with amine groups ($-NH_2$) and carboxylate ions ($COO^-$) to form protonation leading to the more positively charged adsorbent surface. Thus, the adsorption capacity of both MWCNTs-NC and PVA/MWCNTs-NC at lower solution pH decreased mainly because of the electrical repulsion. An increase in adsorption capacity of adsorbents as pH increased might be due to a decrease in competition between $H^+$ and metal cations. Therefore, pH 6.0 was chosen as the optimal pH and used in subsequent adsorption experiments.

*3.2.3. Effect of contact time*

It can be seen from Fig. 4c that the adsorption rates of $Pb^{2+}$ and $Cu^{2+}$ by MWCNTs-NC were very rapid and nearly 100% of $Pb^{2+}$ and 98.6% of $Cu^{2+}$ were removed within 20 min, respectively. While the adsorption of $Pb^{2+}$ and $Cu^{2+}$ onto PVA/MWCNTs-NC increased with the increase of the contact time and the equilibrium was achieved at 90 and 420 min, respectively. Longer equilibrium time was required for PVA/MWCNTs-NC, which may be due to the fact that the immobilization of MWCNTs-NC within the PVA matrix increased mass transfer resistance. The adsorption rates of $Pb^{2+}$ onto MWCNTs-NC and PVA/MWCNTs-NC were significantly higher than those of $Cu^{2+}$, which indicated that MWCNTs-NC and PVA/MWCNTs-NC beads exhibited a strong affinity towards $Pb^{2+}$ ions. $Pb^{2+}$ with a larger ionic radius (1.44 Å) is less hydrated compared to $Cu^{2+}$ (0.74 Å) and less energy is required for dehydration of $Pb^{2+}$ ions to occupy an active site of the adsorbent [23]. Moreover, electronegativity and diffusion coefficient of $Pb^{2+}$ (2.33 and $0.93 \times 10^5$ $cm^2/s$, respectively) are both larger than those of $Cu^{2+}$ (1.90 and $0.71 \times 10^5$ $cm^2/s$, respectively) [24–26]. This can explain the higher adsorption capacity and faster adsorption kinetics for $Pb^{2+}$ compared with $Cu^{2+}$. Therefore, 540 min was chosen as the optimum time for $Pb^{2+}$ and $Cu^{2+}$ adsorption onto PVA/MWCNTs-NC.

*3.2.4. Effect of ionic strength*

The effect of ionic strength on $Pb^{2+}$ and $Cu^{2+}$ adsorption by PVA/MWCNTs-NC was conducted and the results were shown in Fig. 4d. It was found that the increase of the ionic strength from 0.008 to 0.17 mol/L slightly decreased the amounts of $Pb^{2+}$ and $Cu^{2+}$ ions adsorbed onto PVA/MWCNTs-NC. The high ionic strength could compress the double layers at solid/liquid interface, making the surface potential less negative and reducing the activity coefficient of the metal ions in solutions, thus decreasing the binding of metal ions with adsorbents [27]. In addition, $Na^+$ ions could compete with $Pb^{2+}$ and $Cu^{2+}$ ions to react with the active sites and thus decrease the available binding sites for $Pb^{2+}$ and $Cu^{2+}$ ions. Generally, the chemical binding reaction of metal ions with surface functional groups can form the inner-sphere complexes, which were not affected by the change of ionic strength, while the outer-sphere complexes through the weak binding were suppressed by the ionic strength [28]. In this case, PVA/MWCNTs-NC still had considerable adsorption efficiencies for $Pb^{2+}$ and $Cu^{2+}$ ions even at a high concentration of NaCl in solution, indicating that the adsorption mechanism of PVA/MWCNTs-NC for $Pb^{2+}$ and $Cu^{2+}$ ions was mainly chemical adsorption.

*3.2.5. Effect of HA*

Natural organic matters (NOM) are ubiquitously present in the aqueous environment with concentrations up to 10 mg/L [29]. HA the most common organic matter, was selected as the representative of NOM. As shown in Fig. 4d, an increase in HA concentration in solutions slightly decreased the adsorption of $Pb^{2+}$ and $Cu^{2+}$ on PVA/MWCNTs-NC. This is because HA can interact with the active sites and change the physicochemical properties of adsorbent. Meanwhile, the carboxyl and phenolic groups of HA can bind with metal ions through chemical complexation and/or electrostatic interactions. As a result, the adsorption efficiencies of $Pb^{2+}$ and $Cu^{2+}$ were slightly reduced. However, the adsorption efficiencies could still achieve 84% and 58% for $Pb^{2+}$ and $Cu^{2+}$, respectively, even at an HA concentration up to 10 mg/L, which indicated that the affinity of PVA/MWCNTs-NC toward $Pb^{2+}$ and $Cu^{2+}$ was significantly higher than that of HA.

*3.2.6. Effect of temperature*

The influence of temperature on $Pb^{2+}$ and $Cu^{2+}$ adsorption by PVA/MWCNTs-NC was conducted under different temperature from 283 to 313 K. It can be seen from Fig. 5 that the uptake of $Pb^{2+}$ and $Cu^{2+}$ on PVA/MWCNTs-NC slightly decreased when the temperature increased from 283 to 313 K, suggesting that the adsorption process of $Pb^{2+}$ and $Cu^{2+}$ on PVA/MWCNTs-NC was exothermic in nature. Similar results have been reported for metal ions adsorption onto polyacrylonitrile fibers and carbon nanotubes [22,30].

*3.3. Adsorption isotherms*

In present work, Langmuir, Freundlich and Dubinin–Radushkevich isotherms were used to describe the adsorption equilibrium of $Pb^{2+}$ and $Cu^{2+}$ on MWCNTs-NC and PVA/MWCNTs-NC. Langmuir, Freundlich and Dubinin–Radushkevich isotherms can be expressed by Eqs. (2)–(4) [31,32], respectively:

$$\frac{C_e}{Q_e} = \frac{1}{bQ_m} + \frac{C_e}{Q_m} \tag{2}$$

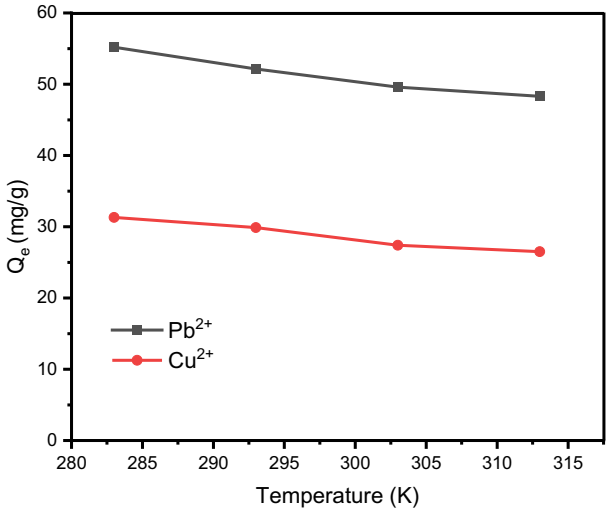


Fig. 5. Effect of temperature on $Pb^{2+}$ and $Cu^{2+}$ onto PVA/MWCNTs-NC.

$$\ln Q_e = \ln K_F + \frac{1}{n}\ln C_e \tag{3}$$

$$\ln Q_e = \ln Q_m - K\varepsilon^2 \tag{4}$$

where $Q_{max}$ is maximum adsorption capacity (mg/g), $b$ is the equilibrium constant (L/mg), $K_F$ is a constant related to the adsorption capacity, $n$ is a constant related to the adsorption intensity, β is a constant related to the mean free energy ($mol^2/J^2$), $Q_m$ is the theoretical saturation capacity (mg/g), ε is the Polanyi potential equal to $RT\ln(1 + 1/C_e)$, $R$ is the gas constant (8.314 J/(mol K)) and $T$ is the absolute temperature (K).

The mean adsorption energy, $E$ (kJ/mol), can be expressed as:

$$E = \frac{1}{\sqrt{-2\beta}} \tag{5}$$

If $E$ value is higher than 8 kJ/mol, the adsorption process takes place chemically and if $E$ value is less than 8 kJ/mol, then the adsorption process takes place physically [33].

Langmuir and Freundlich constants and the correlation coefficients were listed in Table 2. Obviously, the obtained $R^2$ indicated that Langmuir isotherm was more suitable to describe the adsorption equilibrium of $Pb^{2+}$ and $Cu^{2+}$ on MWCNTs-NC and PVA/MWCNTs-NC (also shown in Fig. 6). Therefore, the adsorption process of $Pb^{2+}$ and $Cu^{2+}$ on MWCNTs-NC and PVA/MWCNTs-NC was monolayer adsorption, which was attributed to the homogeneous distribution of active sites on MWCNTs-NC and PVA/MWCNTs-NC. The calculated maximum adsorption capacities ($Q_m$) of MWCNTs-NC and PVA/MWCNTs-NC for $Pb^{2+}$ and $Cu^{2+}$ were 238.10 and 222.22 mg/g, 175.44 and 72.46 mg/g, respectively, which were in good agreement with the experimental values. The Langmuir constant, $b$, was related to the affinity of active sites for metal ions, so the larger values of $b$ indicated the higher affinity of MWCNTs-NC and PVA/MWCNTs-NC for $Pb^{2+}$ ions than $Cu^{2+}$ ions. The $E$ values calculated from Dubinin–Radushkevich isotherm were higher than 8 kJ/mol for both MWCNTs-NC and PVA/MWCNTs-NC, indicating the chemical adsorption involved mechanisms.

### 3.4. Adsorption kinetics

Various kinetics models, namely pseudo-first-order kinetics, pseudo-second-order kinetics, intraparticle diffusion and liquid film diffusion models have been used to describe the experimental data for $Pb^{2+}$ and $Cu^{2+}$ adsorption on PVA/MWCNTs-NC composites. Pseudo-first-order, pseudo-second-order, intraparticle diffusion and liquid film diffusion models can be linearly expressed by Eqs. (6)–(9), respectively:

$$\ln\left(Q_e - Q_t\right) = \ln Q_e - K_1 t \tag{6}$$

$$\frac{t}{Q_t} = \frac{t}{Q_e} + \frac{1}{h} = \frac{1}{K_2 Q_e^2} + \frac{t}{Q_e} \tag{7}$$

$$Q_t = K_{id} t^{0.5} + C \tag{8}$$

$$-\ln(1 - F) = K_{fd} t \tag{9}$$

where $K_1$ (1/min) and $K_2$ (g/(mg min)) are the rate constants of first-order and second-order kinetics, respectively; $Q_t$ (mg/g)

Table 2
Isotherm parameters for $Pb^{2+}$ and $Cu^{2+}$ adsorption onto MWCNTs-NC and PVA/MWCNTs-NC

| Sample | Langmuir | | | Freundlich | | | Dubinin–Radushkevich isotherm | | |
|---|---|---|---|---|---|---|---|---|---|
| | $Q_{max}$ (mg/g) | $K_L$ (L/mg) | $R^2$ | $K_F$ (L/g) | $n$ | $R^2$ | $Q_m$ (mg/g) | $E$ (kJ/mol) | $R^2$ |
| MWCNTs-NC | | | | | | | | | |
| $Pb^{2+}$ | 238.10 | 2.63 | 0.981 | 56.78 | 1.51 | 0.658 | 260.50 | 28.87 | 0.949 |
| $Cu^{2+}$ | 222.22 | 0.36 | 0.988 | 40.33 | 2.12 | 0.847 | 250.08 | 15.08 | 0.915 |
| PVA/MWCNTs-NC | | | | | | | | | |
| $Pb^{2+}$ | 175.44 | 0.27 | 0.998 | 55.45 | 3.99 | 0.952 | 154.92 | 26.73 | 0.936 |
| $Cu^{2+}$ | 72.46 | 0.04 | 0.981 | 17.71 | 4.29 | 0.975 | 59.84 | 16.67 | 0.888 |

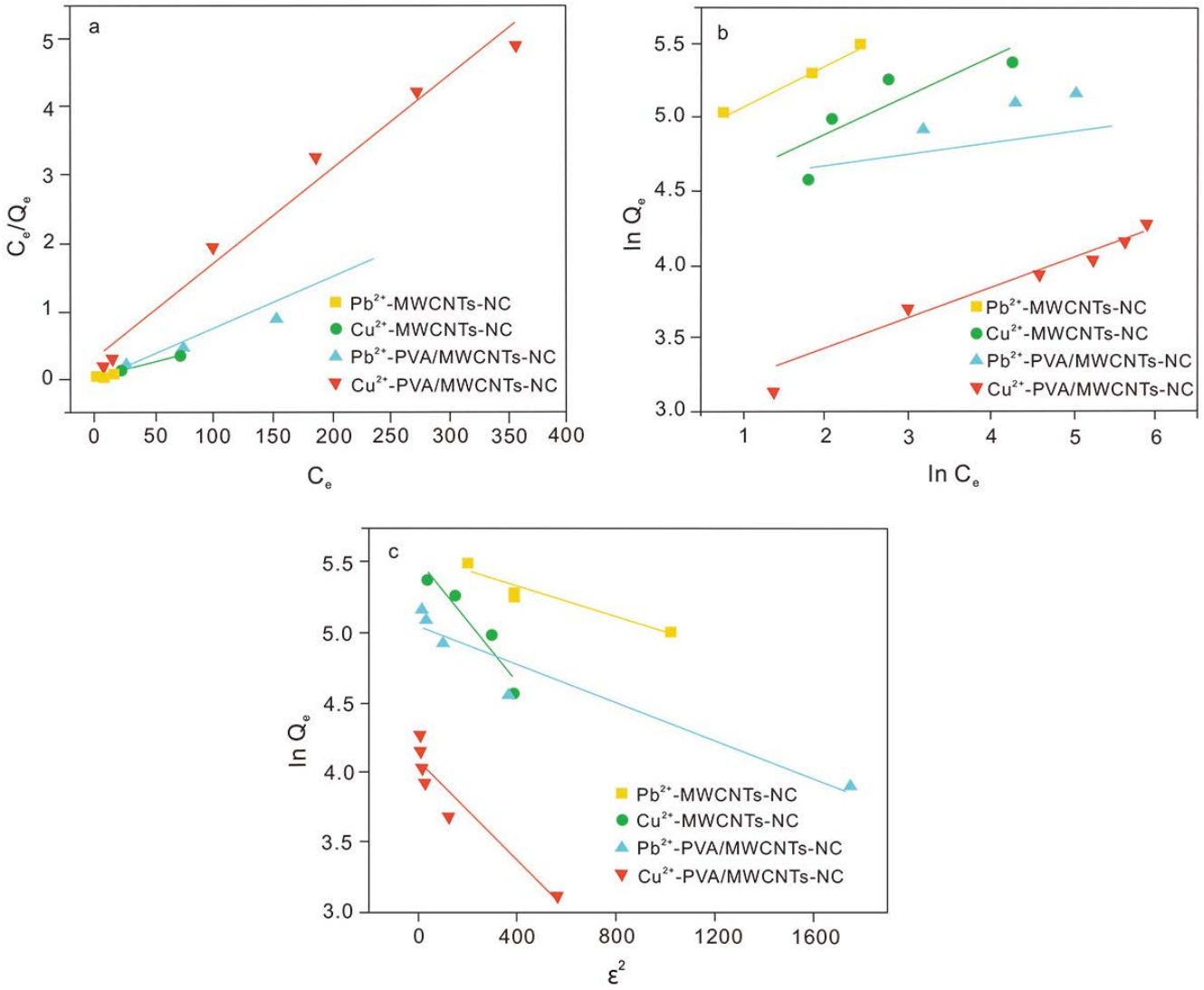


Fig. 6. Langmuir (a), Freundlich (b) and Dubinin–Radushkevich (c) isotherm for $Pb^{2+}$ and $Cu^{2+}$ adsorption by PVA/MWCNTs-NC.

is the adsorption capacity at time $t$ (min); $h$ (mg/(g min)) is the initial adsorption rate; $K_{id}$ is the intraparticle diffusion rate constant (mg/(g $min^{0.5}$)); $C$ is the intercept indicated the boundary layer effect. The larger the intercept value, the greater the contribution of the surface adsorption to the rate-controlling step [12]; $K_{fd}$ is the liquid film diffusion rate constant (1/min) and $F = Q_t/Q_e$. If the plot of $Q_t$ vs. $t^{0.5}$ gave a straight line that passed through the origin, then the intraparticle diffusion was the only rate-limiting step. If the plot of $-\ln(1 - F)$ vs. $t$ showed as a straight line with a zero intercept, the adsorption kinetics was mainly controlled by the film diffusion process.

The linearizing results are shown in Fig. 7 and the parameters are listed in Table 3. According to the correlation coefficient ($R^2$), the kinetic data indicated that the adsorption process was controlled by the pseudo-second-order model. And the calculated $Q_e$ values were very close to the experimental data, which implies that the $Pb^{2+}$ and $Cu^{2+}$ uptake process is due to chemisorption. Moreover, it was obvious that the initial adsorption rate of $Pb^{2+}$ was significantly higher than that of $Cu^{2+}$, which was consistent with the results obtained from a previous investigation of the effect of contact time. The plots of $Q_t$ vs. $t^{0.5}$ showed straight lines with the nonzero intercepts. And the plots of $-\ln(1 - F)$ vs. $t$ also gave the nonzero intercepts for $Pb^{2+}$ and $Cu^{2+}$ adsorption. These results indicated that the film diffusion and the intraparticle diffusion were involved in the adsorption of $Pb^{2+}$ and $Cu^{2+}$. Large intercept values obtained from intraparticle diffusion implied that surface adsorption played an important role in $Pb^{2+}$ and $Cu^{2+}$ adsorption onto PVA/MWCNTs-NC.

### 3.5. Adsorption mechanism

To further obtain insight into the mechanism of $Pb^{2+}$ and $Cu^{2+}$ adsorption on PVA/MWCNTs-NC, XPS spectra of PVA/MWCNTs-NC before and after $Pb^{2+}$ and $Cu^{2+}$ adsorption was analyzed. There were two peaks in N1s spectra for PVA/MWCNTs-NC (Fig. 8a). The binding energy at 400.75 eV could be assigned to the nitrogen atom in –NH

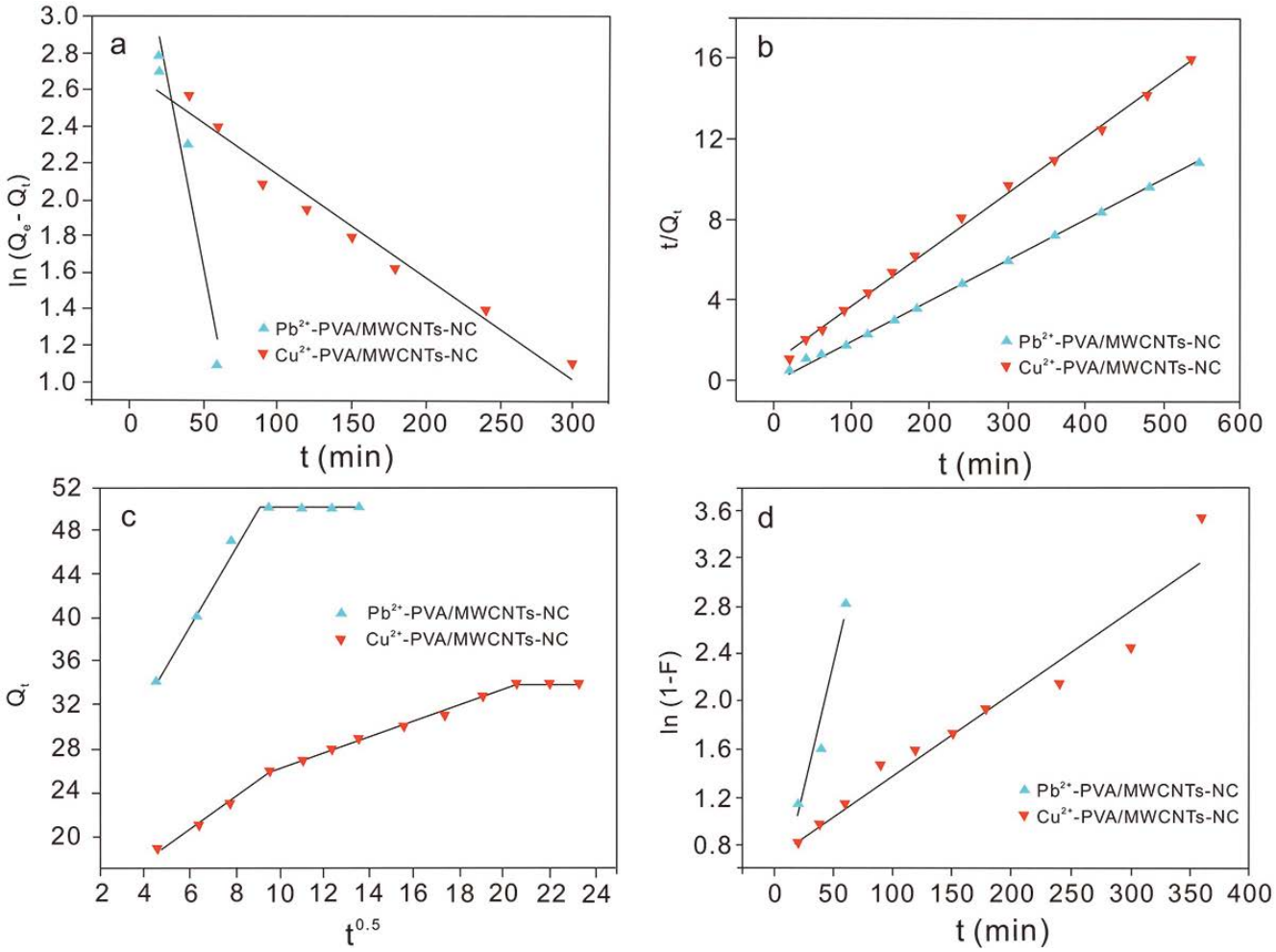


Fig. 7. The pseudo-first-order (a), pseudo-second-order (b), intraparticle diffusion (c) and liquid film diffusion (d) kinetics for $Pb^{2+}$ and $Cu^{2+}$ adsorption by PVA/MWCNTs-NC.

Table 3
Kinetic parameters for $Pb^{2+}$ and $Cu^{2+}$ adsorption onto PVA/MWCNTs-NC

| Metal | Pseudo-first-order | | | Pseudo-second-order | | | | Intraparticle diffusion | | | Film diffusion | |
|---|---|---|---|---|---|---|---|---|---|---|---|---|
| | $Q_e$ | $K_1 \times 10^{-2}$ | $R^2$ | $Q_e$ | $K_2 \times 10^{-3}$ | $h$ | $R^2$ | $K_{id}$ | $C$ | $R^2$ | $K_{fd} \times 10^{-2}$ | $R^2$ |
| $Pb^{2+}$ | 41.75 | 4.18 | 0.939 | 50.50 | 4.21 | 10.75 | 0.999 | 2.61 | 23.83 | 0.904 | 4.18 | 0.939 |
| $Cu^{2+}$ | 16.90 | 0.69 | 0.948 | 35.97 | 0.80 | 1.04 | 0.996 | 0.80 | 17.12 | 0.954 | 0.69 | 0.948 |

groups while 402.61 eV could be attributed to –C–N– groups [13]. As shown in Figs. 8b and c, two new peaks at 402.04 and 400.07 eV were observed after $Pb^{2+}$ and $Cu^{2+}$ adsorption, which could be attributed to the N atoms in the coordination state and the corresponding $Pb^{2+}$ ($Cu^{2+}$) –N complexes formed. In Fig. 8d, the O1s spectrum was divided into three peaks at binding energies of 531.75, 532.65 and 533.51 eV, which could be assigned to C=O, C–O and O=C–O, respectively. However, it was found that the area ratio for the peak at 533.51 eV attributed to the single bond of C–O in carboxylate groups increased from 11.82% to 30.43% and 23.95% after $Pb^{2+}$ and $Cu^{2+}$ adsorption, respectively (Figs. 8e and f). This is because both nitrogen and oxygen atoms possessed lone-pairs of electrons, which could bind to $Pb^{2+}$ and $Cu^{2+}$ through sharing the electron pair and form stable complexes. In Pb 4f spectrum (Fig. 8g), the peaks at 143.72 and 138.87 eV could be ascribed to Pb 4f 5/2 and Pb 4f 7/2, respectively. It was reported that the binding energies of Pb 4f 5/2 and Pb 4f 7/2 in $Pb(NO_3)_2$ were centered at 145.0 and 139.9 eV, respectively [20]. A significant shift to low binding energies was observed after $Pb^{2+}$ adsorption, which might be attributed to the formation of $Pb^{2+}$ –COO– and $Pb^{2+}$ –N complexes [26]. In Cu 2p spectrum (Fig. 8h), two peaks at 933.08 and 934.55 eV were observed,

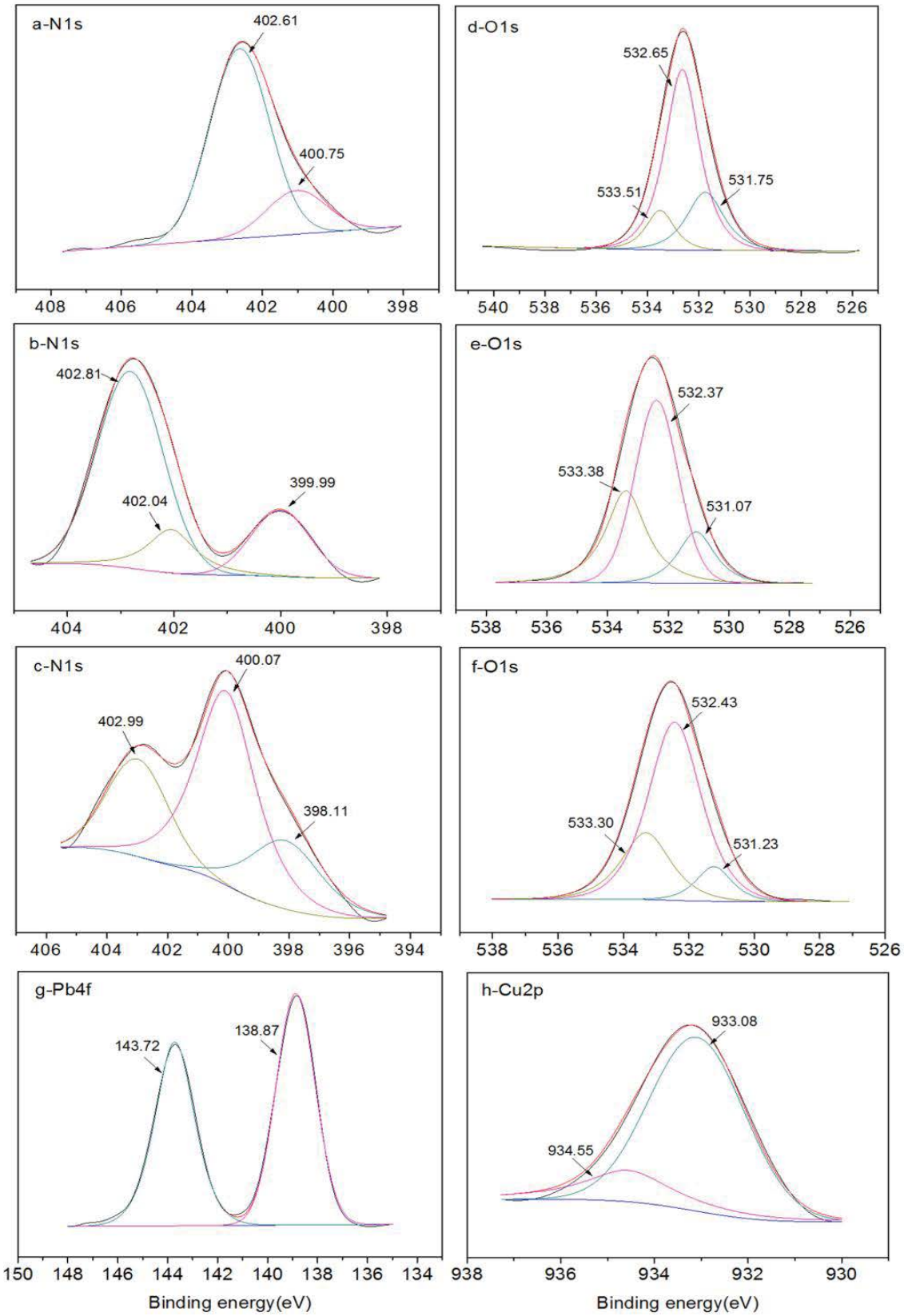


Fig. 8. XPS spectra of N 1s of PVA/MWCNTs-NC (a), $Pb^{2+}$-PVA/MWCNTs-NC (b), $Cu^{2+}$-PVA/MWCNTs-NC (c), O1s of PVA/MWCNTs-NC (d), $Pb^{2+}$-PVA/MWCNTs-NC (e), $Cu^{2+}$-PVA/MWCNTs-NC (f), Pb4f of $Pb^{2+}$-PVA/MWCNTs-NC (g) and Cu4p of $Cu^{2+}$-PVA/MWCNTs-NC (h).

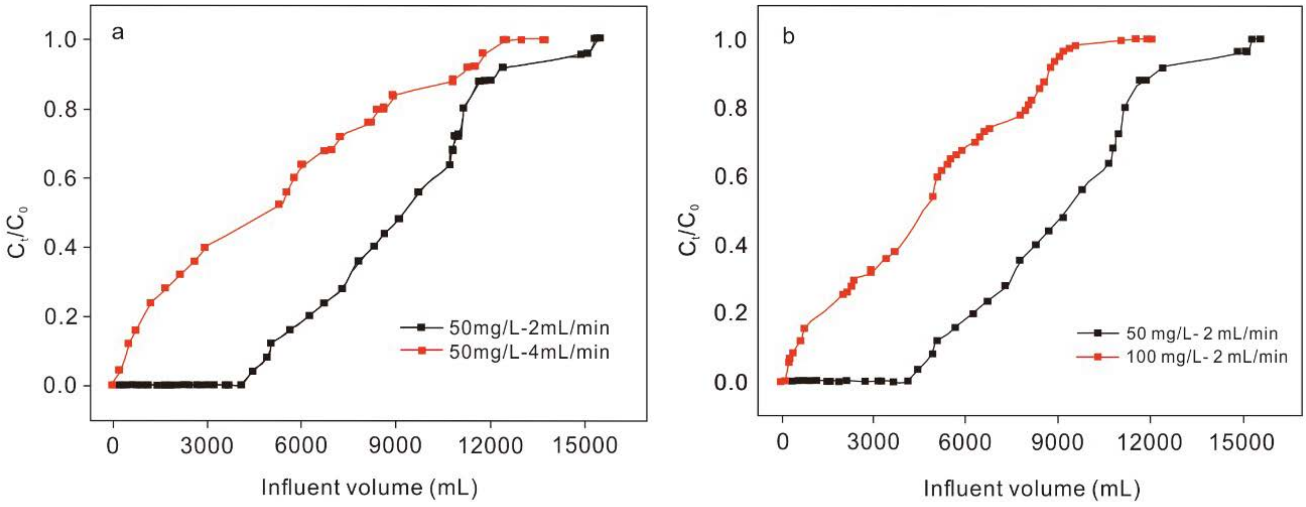


Fig. 9. Breakthrough curves for $Pb^{2+}$ adsorption onto PVA/MWCNTs-NC.

which corresponded to the coordinate binding and ionic binding of $Cu^{2+}$ ions to the functional groups [33]. Based on the FTIR and XPS results, the mechanism of $Pb^{2+}$ and $Cu^{2+}$ adsorption by PVA/MWCNTs-NC was proposed and shown in Fig. 1.

### 3.6. Column studies

The continuous flow operations in column mode were also carried out to evaluate the potential application of PVA/MWCNTs-NC in large-scale wastewater treatment. Some column parameters including the total mass of $Pb^{2+}$ adsorbed ($Q_{total}$, mg), the total amount of $Pb^{2+}$ passed through the column ($M_{total}$, mg), removal percentage ($R$, %) and the equilibrium adsorption capacity ($Q_e$, mg/g) can be determined by Eqs.(10)–(13) [34].

$$Q_{total} = \frac{Q}{1000}\int_{t=0}^{t=t_{total}} C_{ads}dt \tag{10}$$

$$M_{total} = \frac{C_0 \times Q \times t_{total}}{1000} \tag{11}$$

$$R = \frac{Q_{total}}{M_{total}} \times 100 \tag{12}$$

$$Q_e = \frac{Q_{total}}{m} \tag{13}$$

where $C_{ads}$ is the adsorbed metal concentration (mg/L), $C_0$ and $C_e$ are the influent and effluent concentration (mg/L), $Q$ is the flow rate (mL/min), $t_{total}$ is the total time (min) and $m$ is the adsorbent mass (g).

Thomas's model is widely used to describe the fixed-bed adsorption column [34].

$$\frac{C_t}{C_0} = \frac{1}{1+\exp\left(\left(k_{Th}/Q\right)\left(q_{Th}m - C_0V_{eff}\right)\right)} \tag{14}$$

where $k_{Th}$ is the Thomas rate constant (mL/(mg min)) and $q_{Th}$ is the maximum adsorption capacity (mg/g) and $V_{eff}$ is the effluent volume (L).

At a flow rate of 2.0 mL/min (Fig. 9a), the adsorption column containing 2.0 g of PVA/CNTs-NC could purify 4,080 mL of 50 mg/L $Pb^{2+}$ solutions before breakthrough occurred. However, increasing the flow rate from 2.0 to 4.0 mL/min, the breakthrough curves became steeper. At the same time, the breakthrough time and exhaustion time significantly decreased. As an increase in the flow rate reduced the residence time of $Pb^{2+}$ ions in the column, $Pb^{2+}$ ions did not have enough time to diffuse into the interior of adsorbent and react with the active sites, which consequently resulted in lower adsorption capacity and removal efficiency. When the flow rate increased from 2.0 to 4.0 mL/min, the adsorption capacity and the removal efficiencies of $Pb^{2+}$ decreased 123.84 mg/g and 36.21%, respectively.

As shown in Fig. 9b, an increase in $Pb^{2+}$ concentration from 50 to 100 mg/L in influent resulted in a significant decrease in breakthrough time and exhaust time. In a fixed-bed column, the solution with constant $Pb^{2+}$ concentration continuously passed through the column. During this process, $Pb^{2+}$ would be exposed to the limited adsorption sites due to the short contact time. Thus, only a small part of $Pb^{2+}$ ions in the influent could interact with the binding sites and some $Pb^{2+}$ ions were left in the solution. As a result, the breakthrough curve became much steeper. When $Pb^{2+}$ concentration in the influent increased from 50 to 100 mg/L, the adsorption capacity slightly increased, while the removal efficiency decreased by about 20.44%.

Thomas's model exhibited a good fit of the experimental data at a different flow rate and influent metal concentration with high correlation coefficients ($R^2 > 0.977$). The calculated $q_{Th}$ were in agreement with the experimental $Q_{e,exp}$ values. However, the $k_{Th}$ values decreased with increasing the flow rate and influent $Pb^{2+}$ concentration. Thus, the high removal efficiency of $Pb^{2+}$ was obtained at low flow rates and influent metal concentrations. Therefore, decreasing influent metal concentration and the flow rate would result in better utilization of the fixed-bed column.

The adsorption column system showed a higher adsorption capacity of $Pb^{2+}$ in comparison to batch operation. The same results were reported for the biosorption of Cu(II) by the pretreated *Aspergillus niger* biomass in a column [33].

### 3.7. Desorption and reusability

Desorption and reusability of $Pb^{2+}$ and $Cu^{2+}$ loaded PVA/MWCNTs-NC was investigated. $Pb^{2+}$/$Cu^{2+}$ loaded PVA/MWCNTs-NC was added into 20 mL of 0.2 mol/L HCl and shaken for 12 h at room temperature. Then PVA/MWCNTs-NC was placed in 50 mL of 500 mg/L NaCl solution to regenerate. It was found that the HCl solution was quite effective for the desorption of $Pb^{2+}$ and $Cu^{2+}$ ions on PVA/MWCNTs-NC with a high desorption efficiency of 98.8% and 91.3%, respectively. To test the reusability of PVA/MWCNTs-NC, adsorption–desorption operation was repeated 10 times. After 10cycles of adsorption–desorption operations, the concentration of $Pb^{2+}$ and $Cu^{2+}$ in the solution were measured. The results showed that the adsorption efficiency was reduced only by about 10% and 13% for $Pb^{2+}$ and $Cu^{2+}$ ions, respectively, indicating that PVA/MWCNTs-NC had good reusability for $Pb^{2+}$ and $Cu^{2+}$ removal.

## 4. Conclusions

The adsorption experiments showed that succinic anhydride modified MWCNTs (MWCNTs-NC) exhibited excellent adsorption capacities for $Pb^{2+}$ and $Cu^{2+}$ (244 and 215 mg/g, respectively), which were about 40 and 10 times higher than that of pristine MWCNTs. PVA/MWCNTs-NC was able to efficiently remove $Pb^{2+}$ ions at wide pH ranges with rapid kinetics and good selectivity. The adsorption data of $Pb^{2+}$ and $Cu^{2+}$ onto MWCNTs-NC and PVA/MWCNTs-NC fitted Langmuir model well, indicating monolayer adsorption. Kinetic experiments showed that the adsorption of $Pb^{2+}$ and $Cu^{2+}$ onto PVA/MWCNTs-NC followed the pseudo-second-order model suggesting that the surface adsorption and intraparticle diffusion were involved in the adsorption process. FTIR and XPS revealed that complexes were formed between metal ions and functional groups of PVA/MWCNTs-NC. Furthermore, PVA/MWCNTs-NC was reused without significant loss of adsorption capacity after 10 cycles. Thus, it was demonstrated that PVA/MWCNTs-NC showed the good potential for removal of $Pb^{2+}$ and $Cu^{2+}$ ions from effluents.

## Acknowledgment

The authors gratefully acknowledge financial supports from the National Natural Science Foundation of China (Grant No. 21304040), Natural Science Foundation of Gansu Province, China (Grant No.17JR5RA063) and The Water Conservancy Technical Popularization Project of Water Resources Department of Gansu Province, China (Grant No. (2017) 48–14).

## References

[1] Q. Zeng, Y.J. Huang, L.M. Huang, L. Hu, W. Sun, H. Zhong, Z.G. He, High adsorption capacity and super selectivity for Pb(II) by a novel adsorbent: nano humboldtine/almandine composite prepared from natural almandine, Chemosphere, 253 (2020) 126650.

[2] C.P.J. Isaac, A. Sivakumar, Removal of lead and cadmium ions from water using *Annona squamosa* shell: kinetic and equilibrium studies, Desal. Water Treat., 51 (2013) 7700–7709.

[3] L. Sellaoui, D.I. Mendoza-Castillo, H.E. Reynel-Ávila, B.A. Ávila-Camacho, L.L. Díaz-Muñoz, H. Ghalla, A. Bonilla-Petriciolet, A.B. Lamine, Understanding the adsorption of $Pb^{2+}$, $Hg^{2+}$ and $Zn^{2+}$ from aqueous solution on a lignocellulosic biomass char using advanced statistical physics models and density functional theory simulations, Chem. Eng. J., 365 (2019) 305–316.

[4] M. Bodzek, K. Konieczny, A. Kwiecinska-Mydlak, The application of nanomaterial adsorbents for the removal of impurities from water and wastewaters: a review, Desal. Water Treat., 185 (2020) 1–26.

[5] D. Niuniavaite, K. Baltakys, T. Dambrauskas, The adsorption kinetic parameters of $Cu^{2+}$ and $Cr^{3+}$ ions by $\alpha$-$C_2SH$, Desal. Water Treat., 185 (2020) 175–184.

[6] H. Hashtroudi, Treatment of lead contaminated water using lupin straw: adsorption mechanism, isotherms and kinetics studies, Desal. Water Treat., 182 (2020) 155–167.

[7] M.R. Nabid, R. Sedghi, A. Bagheri, M. Behbahani, M. Taghizadeh, H.A. Oskooie, M.M. Heravi, Preparation and application of poly(2-amino thiophenol)/MWCNTs nanocomposite for adsorption and separation of cadmium and lead ions via solid phase extraction, J. Hazard. Mater., 203–204 (2012) 93–100.

[8] L.L. Gao, H.Y. Yin, X.H. Mao, H. Zhu, W. Xiao, D.H. Wang, Directing carbon nanotubes from aqueous phase to o/w interface for heavy metal uptaking, Environ. Sci. Pollut. Res., 22 (2015) 14201–14208.

[9] X.J. Zhou, X.D. Li, S.X. Xu, X.Y. Zhao, M.J. Ni, K.F. Cen, Comparison of adsorption behavior of PCDD/Fs on carbon nanotubes and activated carbons in a bench-scale dioxin generating system, Environ. Sci. Pollut. Res., 22 (2015) 10463–10470.

[10] Y. Cui, S. Liu, Z.J. Hu, X.H. Liu, H.W. Gao, Solid-phase extraction of lead(II) ions using multiwalled carbon nanotubes grafted with tris(2-aminoethyl)amine, Microchim. Acta, 174 (2011) 107–113.

[11] H. Sadegh, G.A.M. Ali, S. Agarwal, V.K. Gupta, Surface modification of MWCNTs with carboxylic-to-amine and their superb adsorption performance, Int. J. Environ. Res., 13 (2019) 523–531.

[12] Y. Cui, Z.J. Hu, J.X. Yang, H.W. Gao, Novel phenyl-iminodiacetic acid grafted multiwalled carbon nanotubes for solid phase extraction of iron, copper and lead ions from aqueous medium, Microchim. Acta, 176 (2012) 359–366.

[13] R.J. Li, X.J. Chang, Z.H. Li, Z.P. Zang, Z. Hu, D.D. Li, Z.F. Tu, Multiwalled carbon nanotubes modified with 2-aminobenzothiazole modified for uniquely selective solid-phase extraction and determination of Pb(II) ion in water samples, Microchim. Acta,172 (2011) 269–276.

[14] Z.P. Zang, Z. Hu, Z.H. Li, Q. He, X.J. Chang, Synthesis, characterization and application of ethylenediamine-modified multiwalled carbon nanotubes for selective solid-phase extraction and preconcentration of metal ions, J. Hazard. Mater., 172 (2009) 958–963.

[15] Y.J. Jin, F. Liu, M.P. Tong, Y.L. Hou, Removal of arsenate by cetyltrimethylammonium bromide modified magnetic nanoparticles, J. Hazard. Mater., 227–228 (2012) 461–468.

[16] J. Huang, M. Ye, Y.Q. Qu, L.F. Chu, R. Chen, Q.Z. He, D.F. Xu, Pb(II) removal from aqueous media by EDTA-modified mesoporous silica SBA-15, J. Colloid Interface Sci., 385 (2012) 137–146.

[17] Y. Sağ, Y. Aktay, Kinetic studies on sorption of Cr(VI) and Cu(II) ions by chitin, chitosan and *Rhizopus arrhizus*, Biochem. Eng. J., 12 (2002) 143–153.

[18] Y. Zhang, Y.F. Li, X.L. Li, L.Q. Yang, X. Bai, Z.F. Ye, L.C. Zhou, L.Y. Wang, Selective removal for $Pb^{2+}$ in aqueous environment by using novel macroreticular PVA beads, J. Hazard. Mater., 181 (2010) 898–907.

[19] A. Idris, N.A.M. Zain, M.S. Suhaimi, Immobilization of Baker's yeast invertase in PVA–alginate matrix using innovative immobilization technique, Process Biochem., 43 (2008) 331–338.
[20] S. Singh, P. Patel, V.K. Shahi, U. Chudasama, $Pb^{2+}$ selective and highly cross-linked zirconium phosphonate membrane by sol–gel in aqueous media for electrochemical applications, Desalination, 276 (2011) 175–183.
[21] R. Thakkar, U. Chudasama, Synthesis and characterization of zirconium titanium phosphate and its application in separation of metal ions, J. Hazard. Mater., 172 (2009) 129–137.
[22] H.Y. Zhu, R. Jiang, L. Xiao, G.M. Zeng, Preparation, characterization, adsorption kinetics and thermodynamics of novel magnetic chitosan enwrapping nanosized γ-$Fe_2O_3$ and multi-walled carbon nanotubes with enhanced adsorption properties for methyl orange, Bioresour. Technol., 101 (2010) 5063–5069.
[23] G.Z. Kyzas, M. Kostoglou, N.K. Lazaridis, Copper and chromium(VI) removal by chitosan derivatives—equilibrium and kinetic studies, Chem. Eng. J., 152 (2009) 440–448.
[24] Y.J. Jia, Y.J. Zhang, R.W. Wang, F.Y. Fan, Q.H. Xu, Studies on adsorptions of metallic ions in water by zirconium glyphosate (ZrGP): behaviors and mechanisms, Appl. Surf. Sci., 258 (2012) 2551–2561.
[25] X.F. Liang, Y.M. Xu, L. Wang, Y.B. Sun, D.S. Lin, Y. Sun, X. Qin, Q. Wan, Sorption of $Pb^{2+}$ on mercapto functionalized sepiolite, Chemosphere, 90 (2013) 548–555.
[26] X.F. Liang, W.G. Hou, Y.M. Xu, G.H. Sun, L. Wang, Y. Sun, X. Qin, Sorption of lead ion by layered double hydroxide intercalated with diethylenetriaminepentaacetic acid, Colloids Surf., A, 366 (2010) 50–57.
[27] A.-H. Chen, S.-C. Liu, C.-Y. Chen, C.-Y. Chen, Comparative adsorption of Cu(II), Zn(II), and Pb(II) ions in aqueous solution on the crosslinked chitosan with epichlorohydrin, J. Hazard. Mater., 154 (2008) 184–191.
[28] E. Repo, J.K. Warchol, T.A. Kurniawan, M.E.T. Sillanpää, Adsorption of Co(II) and Ni(II) by EDTA- and/or DTPA-modified chitosan: kinetic and equilibrium modeling, Chem. Eng. J., 161 (2010) 73–82.
[29] B.J. Pan, H. Qiu, B.C. Pan, G.Z. Nie, L.L. Xiao, L. Lv, W.M. Zhang, Q.X. Zhang, S.R. Zheng, Highly efficient removal of heavy metals by polymer-supported nanosized hydrated Fe(III) oxides: behavior and XPS study, Water Res., 44 (2010) 815–824.
[30] S.B. Deng, R. Bai, J.P. Chen, Aminated polyacrylonitrile fibers for lead and copper removal, Langmuir, 19 (2003) 5058–5064.
[31] J.H. Chen, J.C. Ni, Q.L. Liu, S.X. Li, Adsorption behavior of Cd(II) ions on humic acid-immobilized sodium alginate and hydroxyl ethyl cellulose blending porous composite membrane adsorbent, Desalination, 285 (2012) 54–61.
[32] O. Raize, Y. Argaman, S. Yannai, Mechanisms of biosorption of different heavy metals by brown marine macroalgae, Biotechnol. Bioeng., 87 (2004) 451–458.
[33] M. Mukhopadhyay, S.B. Noronha, G.K. Suraishkumar, Copper biosorption in a column of pretreated *Aspergillus niger* biomass, Chem. Eng. J., 144 (2008) 386–390.
[34] E. Malkoc, Y. Nuhoglu, Fixed bed studies for the sorption of chromium(VI) onto tea factory waste, Chem. Eng. Sci., 61 (2006) 4363–4372.